J. Fluid Mech. (1987), *vol.* 177, *pp.* 485–500
Printed in Great Britain

The effect of spatial restriction on the inner-layer structure of wall turbulence

By SHIGEO MARUYAMA AND HIROAKI TANAKA
Department of Mechanical Engineering, The University of Tokyo,
Bunkyo-ku, Tokyo 113, Japan

(Received 16 October 1985 and in revised form 29 July 1986)

Hot-film-anemometer measurements were carried out in a shear flow between a flat plate and a moving plate fitted with an array of tall fences. The effect of spatial restriction by the fences on the inner-layer structure of the boundary layer developing on the flat-plate side was investigated. It was revealed that the inner-layer structure was maintained even when the tips of the fences were passing at a distance $y^+ = 45$ from the flat plate; the flow did not become laminar-like until the tips reached $y^+ = 25$. These results suggested the physical view that the inner layer of wall turbulence has a tough, self-sustaining structure, which is uniquely determined under a given mean wall shear stress and is hardly influenced by outer-layer disturbances provided that its own spatial extent of about $45\,\nu/u^*$ from the wall is maintained.

1. Introduction

Kline *et al.* (1967) investigated the region very close to the wall in turbulent boundary layers using the hydrogen-bubble technique. They observed low-speed streaks distributed randomly in space and time, which occasionally lifted up from the wall, and then, with sudden oscillation, mixed violently with the higher-momentum fluid farther from the wall. They called this violent mixing 'bursting'.

It was discovered that such a coherent motion near the wall also existed in turbulent pipe flow (Corino & Brodkey 1969) and in channel flow (Wallace, Eckelmann & Brodkey 1972; Brodkey, Wallace & Eckelmann 1974), and thus it was confirmed to be a phenomenon common to all wall-bounded turbulence. Soon afterwards, it was discovered that the generation of Reynolds stress was associated with this coherent motion. Namely, the highly intermittent nature of the Reynolds stress was found by examining the probability density distribution of the instantaneous uv signals by Gupta & Kaplan (1972) and recently by Andreopoulos *et al.* (1984); then a close relation between the coherent motion and instantaneous production of the Reynolds stress was perceived by means of flow visualizations by Corino & Brodkey (1969), Kim, Kline & Reynolds (1971) and others, as well as with the aid of various data processing methods by Wallace *et al.* (1972), Brodkey *et al.* (1974), Willmarth & Lu (1972), and Blackwelder & Kaplan (1976). Stimulated by these findings, many researchers over the last decade have been studying the mechanism of the coherent structure in the wall region. The latest review is available in Hirata *et al.* (1982).

Bakewell & Lumley (1967) suggested the existence of counter-rotating eddy pairs aligned in the streamwise direction with their centres at about $y^+ = 30$ ($y^+ = yu^*/\nu$, where y is distance from the wall, u^* the friction velocity, ν the kinematic viscosity) as a physically possible cause of the low-speed streaks appearing very close to the

wall. Experimental support was given to this suggestion by Blackwelder & Eckelmann (1979), who investigated the wall region using an oil channel to obtain a thick viscous sublayer, and measured the streamwise and spanwise velocity components as well as the gradients of these components in the vertical direction. Both the quadrant probability analysis and the conditional-sampling technique utilizing variable-interval-time-averaged (VITA) fluctuation energy were introduced, and the existence of the counter-rotating eddy pairs with their centres at $y^+ = 20$–30 was indicated. Later, Blackwelder (1983) examined the conditionally averaged spanwise velocity profiles and suggested that the vertical extent of these eddy pairs should reach $y^+ = 50$.

The spanwise spacing of the low-speed streaks λ has been fairly well estimated from flow visualizations such as the hydrogen-bubble technique (Kline *et al.* 1967; Smith & Metzler 1983), dye seeping (Oldaker & Tiederman 1977) and others (Corino & Brodkey 1969), as well as from probe methods such as measuring correlations between the outputs of wall sensors separated in the spanwise direction (Meek & Baer 1970; Lee, Eckelman & Hanratty 1974; Kreplin & Eckelmann 1979). Smith & Metzler (1983) demonstrated that the probability distribution of the foregoing spacing data merged into a single curve, irrespective of the Reynolds number, when non-dimensionalized by the viscous lengthscale ν/u^*, with their mean and mode amounting to $100\,\nu/u^*$ and $(75$–$80)\,\nu/u^*$ respectively.

On the other hand, the streamwise length of the low-speed streaks Δx has not yet been well investigated. Based on the longitudinal correlations of wall-probe outputs (Meek & Baer 1970; Kreplin & Eckelmann 1979), instantaneous two-dimensional-pattern measurements of pressure fluctuations at the wall surface (Dinkelacker *et al.* 1977), and a visualization study using a thermo-sensitive liquid-crystal (Iritani, Kasagi & Hirata 1983), it is suspected that the streamwise length Δx may exceed $1000\,\nu/u^*$.

It seems generally agreed that the foregoing counter-rotating eddy-pair structure causes the so-called 'ejection' of low-speed fluid outward from the wall as well as the 'sweep' of high-speed fluid coming down to the wall, and that these intermittent 'events' make large contributions to the Reynolds stress.

Rao, Narasimha & Badri Narayanan (1971) and Laufer & Badri Narayanan (1971) reported that the mean period between the successive events became independent of the Reynolds number when non-dimensionalized by the outer-flow timescale δ/U_∞ (U_∞ is free-stream velocity, δ the boundary-layer thickness). This stimulated speculation about the relation between the events in the wall region and the large-scale structure in the outer layer (Laufer & Badri Narayanan 1971; Brown & Thomas 1977; Falco 1977; Fleischmann & Wallace 1984). On the other hand, some reports insisted that the period of events should scale with the viscous timescale ν/u^{*2}. Meek (1972) calculated, on the basis of the surface-renewal model, the mean period T needed for the viscous sublayer to grow to a certain size. He showed that this value became almost constant at $T^{+\frac{1}{2}} = (Tu^{*2}/\nu)^{\frac{1}{2}} = 15$ irrespective of the Reynolds number and suggested that this period might explain the bursting period. Blackwelder & Haritonidis (1983) indicated the strong effect of the sensor size on the bursting-period measurement and recommended that a period measured with a sensor of length l less than $20\,\nu/u^*$ would be free from the spatial-averaging effect. Then, without the spatial-averaging effect, the period of events scaled with the viscous timescale and was $T^+ = 300$ irrespective of the Reynolds number. Willmarth & Sharma (1984), using a very small sensor of $l^+ = 0.3$, achieved similar results to Blackwelder & Haritonidis (1983).

So far, experimental studies have been performed on boundary layers, pipes, and channels, with special attention to keeping the flow in the fully developed state so as not to introduce any disturbance. In such ideally developed conditions, the inner layer of wall turbulence interacts in a natural manner with the outer layer or the core region, and vice versa. Since the structure of either layer has not been well understood, discussions about the interaction between the two layers as well as their independence cannot help becoming vague. This paper places its focus on the inner-layer structure. An experiment is described in which large artificial disturbances are introduced deep into the outer layer. This may be considered as providing the inner layer with artificial boundary conditions. By examining the influence of these disturbances on the inner layer, we attempt to reveal some aspects of the physical mechanism of the so-called coherent structure in the inner layer.

In practice, a Couette-like shear flow is realized between a flat plate and a moving plate fitted with an array of tall fences. The effect of the disturbance by the fences on the inner-layer structure of the boundary layer developing on the flat-plate side is investigated with hot-film anemometry by changing systematically the relative configuration of the fences. As a result, the strong independence of the inner-layer structure and also the spatial extent needed to maintain the structure will be demonstrated.

2. Experimental apparatus and procedure

Figure 1 shows the experimental apparatus. In an open water tank made of Plexiglas 2 m long, 1 m wide, and 0.44 m deep, a plate fitted with an array of fences moves horizontally. A speed-variable 200 W motor equipped with a reduction gear and a timing-belt and pulley set are arranged outside the tank and drive a pair of stainless-steel sprocket wheels inside the tank through a shaft penetrating the tank wall. The sprockets carry stainless-steel conveyor chains, which slide smoothly along horizontal aluminium guide rails supported by synthetic-resin rollers. Fifty-eight Plexiglas fence elements, with a T-shaped cross-section (figure 2) of 614 mm effective length, are bolted at their both ends to each link of the conveyor chains so that they constitute the moving plate fitted with an array of fences. Between this moving plate and a flat Plexiglas upper plate, a Couette-like shear flow is established. The width of the flow field is 620 mm, bounded by the side plates.

The distance from the flat plate to the tips of the fences h, the pitch of the fences p, and the velocity of the moving plate U_c (see figure 2) were varied over the following ranges: 5 mm $\leqslant h \leqslant$ 20 mm, $p = 63.5$ and 127 mm (every other fence element was overturned), and 16.7 mm/s $\leqslant U_c \leqslant$ 196 mm/s respectively.

The measuring station is 1260 mm downstream from the inlet end. Figure 2 shows the details of the measuring station. The instantaneous streamwise velocity was measured with a quartz-coated platinum hot-film probe which could be made to traverse the space between the flat plate and the tips of the fences by a micrometer head. As shown in figure 2, the traversing mechanism is fixed to a thick Plexiglas disk 230 mm in diameter, the under surface of which is devised to be mounted flush with the main flat plate. For determining the initial position of the probe, the measuring station, together with the bottom disk, was taken out of the apparatus and settled upside down on a rest stand. The hot-film probe was moved so close to the wall that the tips of the prongs almost touched it. Using a microscope, equipped with a dial gauge for measurement of vertical position, we focused its cross-hairs first on the sensing wire of the probe and then on its reflected image on the wall. Dividing

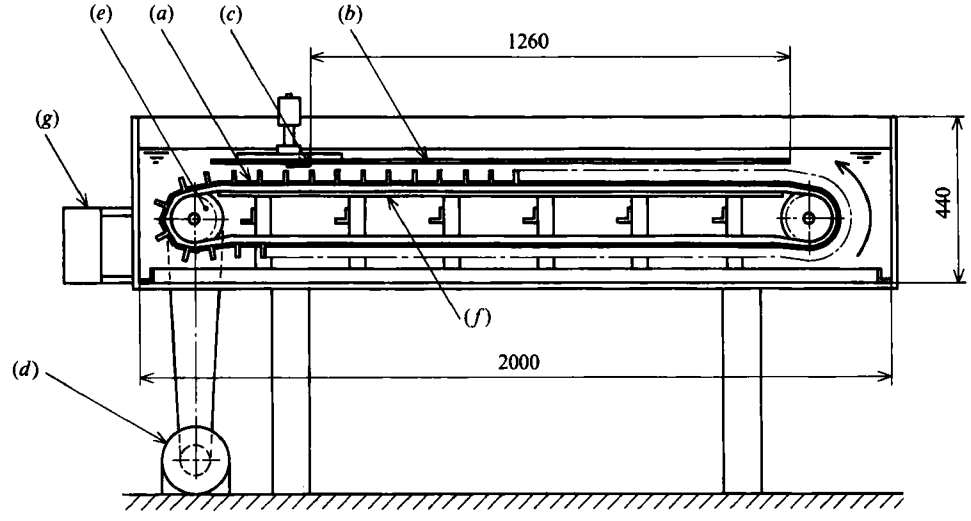

FIGURE 1. Experimental apparatus: (*a*) moving plate fitted with an array of tall fences, (*b*) upper flat plate, (*c*) measuring station, (*d*) motor, (*e*) driving sprocket, (*f*) horizontal guide rail, (*g*) filter system. Dimensions in mm.

the displacement between the two positions of the microscope by two, we could determine the initial distance of the sensor from the wall with an accuracy of ± 20 μm. When we examined the near-wall region, the probe was mounted with its shank deflected toward the flat plate by a small angle of about 7° from the horizontal (see figure 2) in order to make it possible for the sensor to be set very close to the wall. But, when we examined the region far from the wall (i.e. $y \geqslant 5$ mm), the probe was mounted so that its shank was inclined slightly away from the flat plate.

Probe interference effects may be suspected because the geometry of the flow field relative to the sensor seems complex at first glance. However, the mean flow direction was considered to be parallel to the wall despite the existence of the fences, and the prongs and the shank of the hot-film probe were located downstream to the sensor. So, the probe interference effect did not seem to be large. Furthermore, the main series of experiments were carried out using a miniature probe (TSI model 1260–10W) with shank diameter as small as 1.5 mm. In the remaining experimental series, a larger probe with a shank diameter of 3.2 mm (TSI model 1210–60W) was used, and similar results were obtained also in this case (see table 1 for the experimental series and the probe used).

Calibration of the hot-film probe was made in a rotating cylindrical vessel, before and after every one-day experiment. This vessel was 190 mm in inner diameter and 200 mm high. The speed of revolution was regulated over a range of 0.5–78 r.p.m., using a speed-variable motor and two sets of reduction gears. After the vessel had begun to rotate at a constant speed, more than ten minutes were required for the solid rotation of water in the vessel to be established. During this period, the hot-film probe was submerged but was held at the centre of the vessel. Then, it was moved to the specified position for calibration, 70 mm from the axis of rotation. An immediate output of the anemometer was recorded before the probe had affected the solid rotation of water.

A hot-film anemometer KANOMAX SYSTEM 7000 (licensed by TSI) was run at an over-heat ratio of 5%. The output signal underwent primary linearization by an

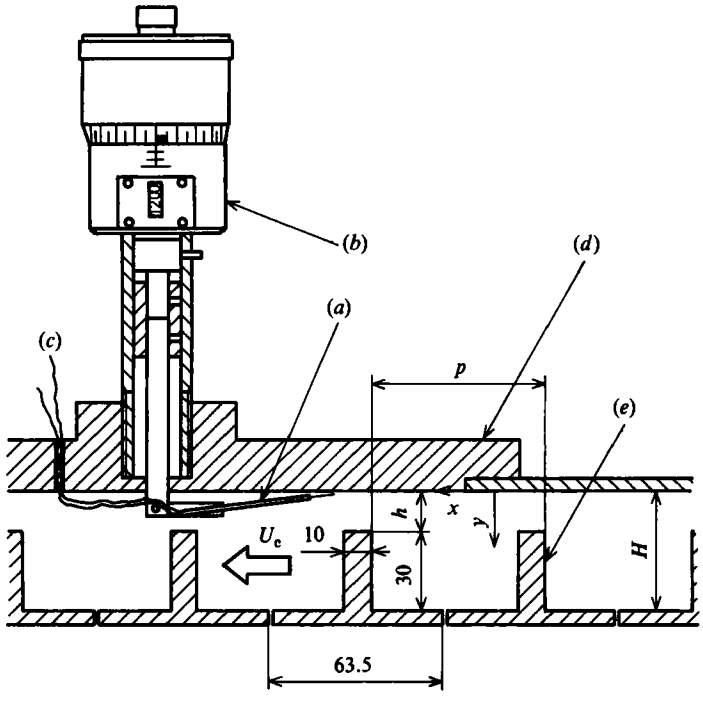

FIGURE 2. Details of measuring station: (*a*) hot-film probe, (*b*) micrometer head, (*c*) lead wires to anemometer, (*d*) demountable portion of upper plate, (*e*) a fence element. Dimensions in mm.

analogue linearizing circuit under fixed controller parameters without fine adjustment, leaving more accurate linearization to digital processing as mentioned below. The water temperature variation was compensated based on the output of the temperature-compensator circuit using a platinum-resistance thermometer. The primary-linearized and temperature-compensated output signals at the time of the velocity calibration as well as of the main experiment were recorded on analogue magnetic tapes by a data recorder TEAC R210A.

The recorded analogue data were digitized with a 12 bit A/D converter controlled by a minicomputer MELCOM 70/30C. All data processing was done on this computer. A polynominal of the third order provided least-squares fit for an ultimate linearization on the computer. Mean velocity, turbulent intensity, power spectrum, and other statistical quantities were calculated and plotted by the computer. The digitizing interval T_s at A/D conversion was varied according to each experimental run (examples are shown in table 2 for series F236). In most cases, T_s was taken to be less than one half of the viscous timescale ν/u^{*2}; and 16384 digitized data points were inputted for a single data reduction. Thus, from the Nyquist sampling theorem, the power spectrum obtained by the FFT algorithm should be valid over the frequency range of four decades with the upper bound extending beyond the frequency u^{*2}/ν, which covers well the important frequency range concerned in the wall turbulence (see figure 8).

Since the thermal conductivity of Plexiglas is less than half that of water, a slight decrease in the anemometer output was detected when the sensor came very close to the wall in still water. However, this decrease was negligible for the present velocity measurements made within the range $y \geqslant 0.2$ mm. In order to keep the water clean

Series	h (mm)	p (mm)	Range of U_c (mm/s)	Range of u^* (mm/s)	Probe (TSI model)
F315	20	63.5	30.9–196	1.53–9.56	1210–60W
F236	15	63.5	35.2–99.7	1.61–5.25	1260–10W
F118	15	127	29.9–101	1.44–5.00	1260–10W
F039	5	127	16.7–158	1.61–11.7	1210–60W
Channel	7.5	—	4240	233	5 μm tungsten hot-wire

TABLE 1. Experimental series. 'Channel' is reference data for air flow in a channel (Tanaka & Yabuki 1986), and h and U_c are half the channel height and the centreline velocity respectively.

enough to ensure that the hot-film anemometry did not drift, the water was first degassed by heating up to 60 °C and then fed to the tank through a filter system which could catch particles of dirt larger than 1 μm. Furthermore, the water was continuously circulated through the filter system at a rate of 11 l/min during the experiment. The water temperature variation through any one-day experiment was not greater than 1.6 °C. As a result, the drift of the anemometer output was kept to within ± 2–3 % through each one-day experiment. Taking account of other causes of errors, the resultant uncertainty involved in the measured mean velocity was estimated to be ± 5 % (20:1).

3. Results

Four series of experiments were carried out as listed in table 1. In each series, the moving-plate velocity U_c was varied under a fixed combination of the distance between the wall and the fence tips h and the fence pitch p. (The numerical part of the series name denotes 1000 times h divided by p.) Table 1 also gives the corresponding changes of the friction velocity u^*, the experimental determination of which is explained in §3.1. The series labelled 'channel' is the air-flow data in a two-dimensional channel obtained by Tanaka & Yabuki (1986), which will appear in the later sections as reference data. If the fences were removed from the present experimental apparatus, a pure Couette flow would be realized, which would seem more suitable for comparison. However, we are not simply studying the particular inner-layer structure in the Couette flow of water but are interested in the inner-layer structure common to all wall turbulence of any fluid. Thus we consider the fully developed air-flow data in a channel to be the most appropriate reference data for wall turbulence that we have to hand in the form of an analogue magnetic tape.

The experimental results for series F236 ($h = 15$ mm and $p = 63.5$ mm) are picked out from the four series and are shown in figures 4–8. The experimental conditions for that series are listed in table 2. As the moving-plate velocity U_c is varied, the friction velocity u^* changes roughly in proportion to U_c, resulting in corresponding changes in the viscous lengthscale ν/u^* as well as in the viscous timescale ν/u^{*2}. In the second and third columns of table 2, h and p are non-dimensionalized as $h^+ = hu^*/\nu$ and $p^+ = pu^*/\nu$ respectively. If the coherent structure in the inner layer of wall turbulence scales with the viscous lengthscale, a set of h^+ and p^+ may serve as the parameters that represent the spatial restriction on the inner-layer structure; that is, if the experimental system is transformed into the non-dimensional coordinates (x^+, y^+, z^+) with the flat-plate surface being coincident with the (x^+, z^+)-plane,

Run No.	h^+	p^+	U_c (mm/s)	u^* (mm/s)	$Re_h = hU_c/\nu$	ν/u^* (mm)	ν/u^{*2} (ms)	T_s (ms)
F236:1	20.7	87.8	35.2	1.61	454	0.723	450	32
F236:2	31.5	133	48.9	2.35	654	0.477	203	32
F236:3	37.2	158	60.0	2.86	782	0.403	141	32
F236:4	49.3	209	72.3	3.65	977	0.304	83.5	12.8
F236:5	56.9	241	85.0	4.21	1150	0.263	62.6	9.6
F236:6	71.0	300	99.7	5.25	1350	0.211	40.3	6.4
Channel	113	—	4240	233	2070	0.0661	0.284	0.1

TABLE 2. Experimental conditions for series F236 (h = 15 mm and p = 63.5 mm). For channel flow refer to table 1.

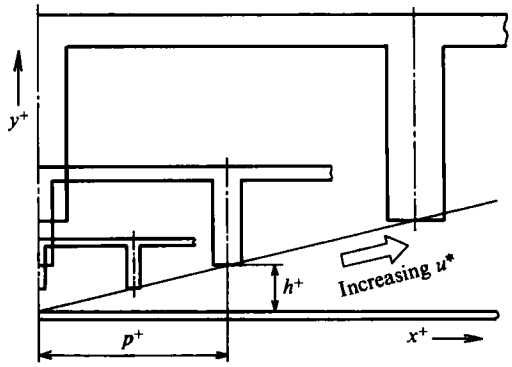

FIGURE 3. Arrangement of the experimental system in non-dimensionalized coordinates.

and if the tip of one fence is at $x^+ = 0$ and $y^+ = h^+$, then the tip of the preceding fence is at $x^+ = p^+$ and $y^+ = h^+$ (figure 3). Thus the space that the coherent structure can occupy would be restricted by h^+ in the vertical direction and by p^+ in the streamwise direction. When u^* changes with increasing U_c under a fixed combination of h and p, the arrangement of the flat plate and the fences in the non-dimensionalized space changes merely in size, as shown in figure 3. In the range of the present experiment, however, h^+ seemed to be a more important parameter than p^+. So, h^+ was chosen as the chief parameter to represent the experimental conditions in the later sections.

Two kinds of Reynolds numbers may be defined. One is based on the gap h and the translating velocity U_c. This Reynolds number Re_h is given in table 2. Indeed, it does not strictly correspond to any Reynolds number defined in the boundary-layer flow or in the channel flow. But h is considered primarily to represent the shear-layer thickness, suggesting its correspondence to the boundary-layer thickness or to half the channel height, while U_c is approximately equal to the velocity difference across the shear layer (see figure 4), corresponding to the free-stream velocity or to the centreline velocity in the channel flow. Considered in this way, the range of Re_h in table 2 seems rather small. This, however, results directly from the nature of the present investigation. And, the minimum Re_h at which turbulence would be maintained is the question at issue.

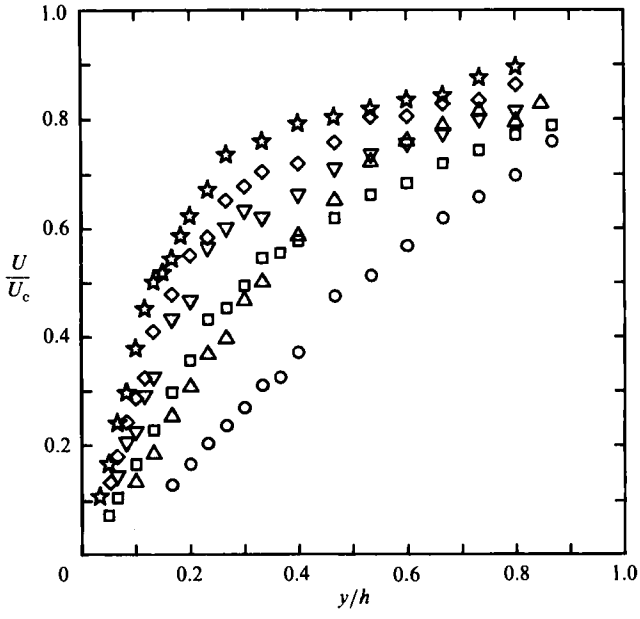

FIGURE 4. Mean streamwise velocity profiles for F236 (h = 15 mm and p = 63.5 mm). ○, h^+ = 20.7; △, 31.5; □, 37.2; ▽, 49.3; ◇, 56.9; ☆, 71.0.

Another Reynolds number Re_H can be defined using the distance H between the two plates (see figure 2) and the translating velocity U_c. This Reynolds number can be easily calculated from Re_h, i.e. $Re_H = 3Re_h$ in the case of series F236 where h = 15 mm and H = 45 mm. The magnitude of Re_H is considered to reflect the likelihood of the flow becoming turbulent without the spatial restriction of the fences. From this point of view, the ideal apparatus would have the ratio H/h as large as possible. Judging from the results described in the later sections, however, the geometry of the present experimental apparatus was fairly successful in maintaining turbulence down to sufficiently small Re_h to accomplish the real objective of the present investigation.

With respect to the development of the flow, the vertical lengthscale over which the shear layer must diffuse to develop is approximately h, which is smaller than H. Then the entrance region may be somewhat shorter than expected on the basis of the distance between the two plates. Moreover, the flow is subjected to successive tripping by the fences, which ensures the steady development of the turbulent flow. Thus the flow is considered to be fully developed at the measuring station located more than 60 h downstream from the inlet. This is well demonstrated by the measured velocity and turbulent intensity distributions in the following sections. Namely, both profiles for the case of the largest h^+ agree well with the standard wall-turbulence profiles.

3.1. *Mean velocity profiles*

Figures 4 and 5 show the time-averaged velocity profiles. Figure 4 is on a linear scale, and the mean velocity U and the distance from the wall y are normalized by U_c and h respectively. In figure 5, the velocity profiles are made dimensionless with the wall variables to be compared with the universal velocity profile. The friction velocity was

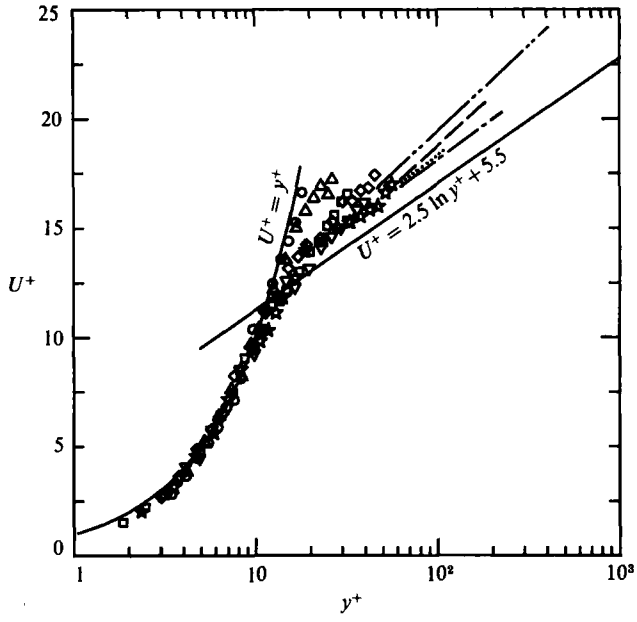

FIGURE 5. Mean streamwise velocity profiles in 'law-of-the-wall' coordinates for F236 ($h = 15$ mm and $p = 63.5$ mm). ○, $h^+ = 20.7$; △, 31.5; □, 37.2; ▽, 49.3; ◇, 56.9; ☆, 71.0; ·····, Tanaka & Yabuki (1986); – – –, Kline *et al.* (1967); — · —, Eckelmann (1974); — · · —, Blackwelder & Haritonidis (1983).

obtained from the velocity gradient near the wall by fitting the data to the linear profile. The velocity profile in the case of a low Reynolds number seems to deviate slightly upward from the straight line in the figure, $U^+ = 2.5 \ln y^+ + 5.5$. Besides the reference data for channel flow of Tanaka & Yabuki (1986), three other examples are plotted in the figure; boundary-layer flows without a pressure gradient from Kline *et al.* (1967), two-dimensional channel flows from Eckelmann (1974), and boundary-layer flows from Blackwelder & Haritonidis (1983). Here, we should note that the friction velocity of all the cited data has been obtained from fitting the mean velocity data to the linear profile near the wall.

The present experimental profiles for h^+ greater than 45, collapsing together, seem to obey the law of the wall. As h^+ decreases below 40, the measured velocity distribution departs from the universal profile and tends continuously to the laminar profile, $U^+ = y^+$. When $h^+ = 20.7$, the measured profile becomes almost linear (see also figure 4).

3.2. *Streamwise turbulent intensities*

Streamwise turbulent-intensity distributions are shown in figure 6, together with the reference data by Tanaka & Yabuki (1986) and two recent measurements at relatively low Reynolds numbers. Andreopoulos *et al.* (1984) investigated the influence of the Reynolds number on the characteristics of turbulent boundary layers. The solid line in figure 6 is a reproduction of their data for the lowest Reynolds number of $Re_\theta = \theta U_\infty/\nu = 3624$, where U_∞ is the free-stream velocity and θ the momentum thickness. The broken line is the channel data of Alfredsson & Johansson (1984) at $Re_h = hU_c/\nu = 7500$, where h is half the channel height and U_c is the centreline velocity. Johansson & Alfredsson (1983) have pointed out that the peak value of the

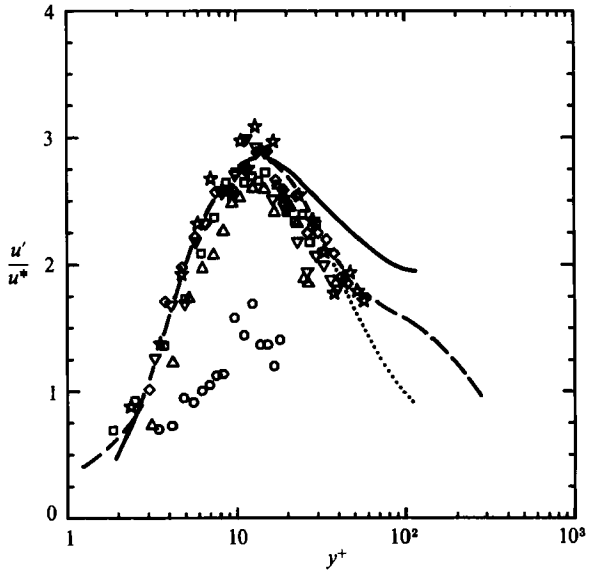

FIGURE 6. Streamwise turbulent-intensity distributions for F236 (h = 15 mm and p = 63.5 mm). ○, $h^+ = 20.7$; △, 31.5; □, 37.2; ▽, 49.3; ◇, 56.9; ☆, 71.0; ·····, Tanaka & Yabuki (1986); ——, Andreopoulos *et al.* (1984), boundary layer, $Re_\theta = \theta U_\infty/\nu = 3624$; – – –, Alfredsson & Johansson (1984), channel, $Re_h = hUc/\nu = 7500$.

turbulent-intensity distribution shows a decreasing tendency with increasing sensor length because of the imperfect spatial resolution. The effective length of the present sensor is 1 mm. This is equivalent to 1.4–4.7 viscous units for the experimental conditions in figure 6, and proves to be small enough to attain the highest peak value.

The measured distributions for h^+ greater than 35 merge with the previous data in the region of y^+ less than 15, including the point of the highest intensity. It is surprising that even in the case where $h^+ = 37.2$, which means the tips of the fences are passing at a distance $y^+ = 37.2$ from the flat plate, the intensity profile is almost the same as the fully developed wall turbulence. When $h^+ = 31.5$, the intensities become slightly smaller than the developed turbulence. Considerably lower intensities are obtained in the case of $h^+ = 20.7$. Under this condition, it seems that the turbulence structure cannot be maintained any longer and the flow becomes laminar-like.

3.3. *Instantaneous streamwise velocity signals*

The instantaneous velocity signals at $y^+ = 15$, including that of the reference data for channel flow of Tanaka & Yabuki (1986), are shown in figure 7. In the figure, time t is non-dimensionalized by the viscous timescale ν/u^{*2}, and the velocity fluctuation u by the friction velocity. Comparing the signal for a large h^+ such as 56.9 or 71.0 with the channel flow signal, it can be observed that they are quite alike except for their high-frequency components. On the other hand, the signal for $h^+ = 20.7$ is entirely different. The long-term fluctuations vanish and pulse-like fluctuations of high frequency become conspicuous. The period between successive pulses is found to correspond to the time interval at which the successive fences pass the measuring station. This time interval T_p, non-dimensionalized in the same manner as t in the

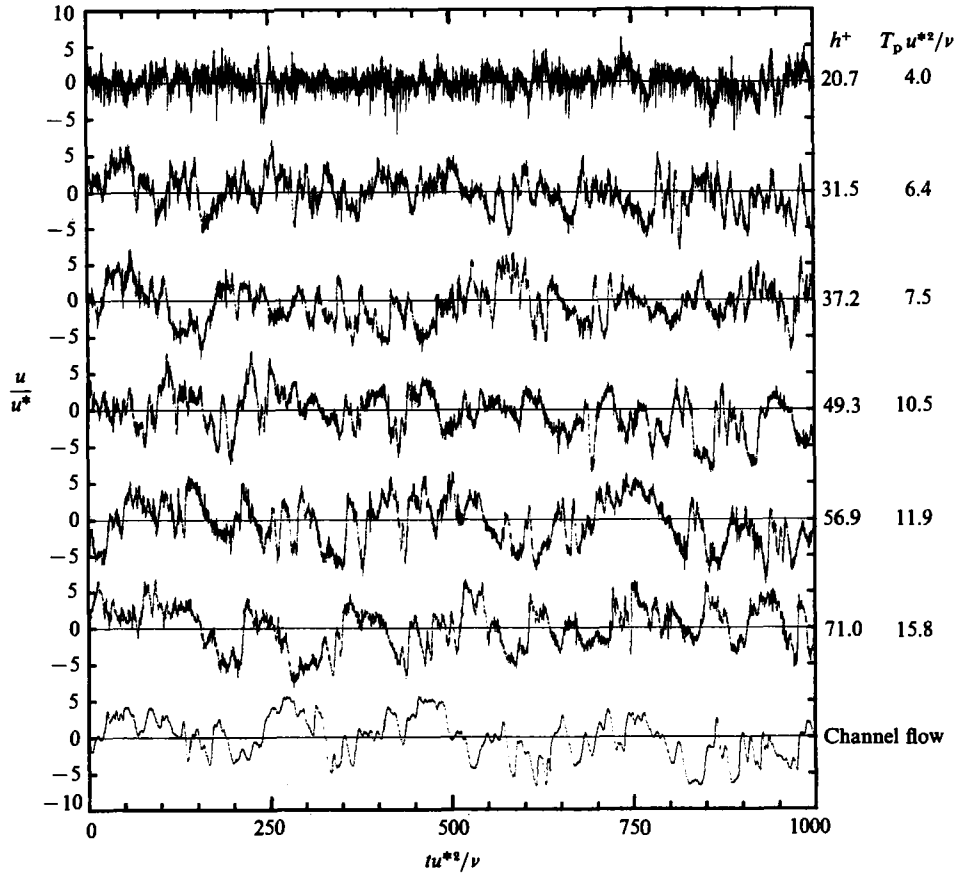

FIGURE 7. Instantaneous streamwise velocity signals at $y^+ = 15$ for F236 ($h = 15$ mm and $p = 63.5$ mm).

abscissa, is shown on the right-hand side of figure 7. Moreover, it was confirmed with the aid of an oscilloscope that the pulse was generated at almost every instant when the tip of the fence exactly passed the sensor position. Though small in magnitude, pulse-like fluctuations that keep pace with the passage of the fences are discernible in the signals for larger h^+, even for $h^+ = 56.9$ and 71.0.

The signals for $h^+ > 30$ show no significant features other than the superposition of the foregoing pulse-like fluctuations which, having negligible energy, seem to represent no essential change in the main structure of the flow (see §3.4). A quite sudden decrease of the long-term main fluctuations occurs when the gap h^+ decreases below 25.

3.4. *Spectra of streamwise velocity fluctuations*

Figure 8 shows the power spectra of the velocity fluctuations at $y^+ = 15$, again together with that of the channel flow. The frequency f is non-dimensionalized by the viscous timescale ν/u^{*2}, and the power spectral density $E(f)$ is made dimensionless so that the integral with respect to the logarithm of non-dimensional frequency

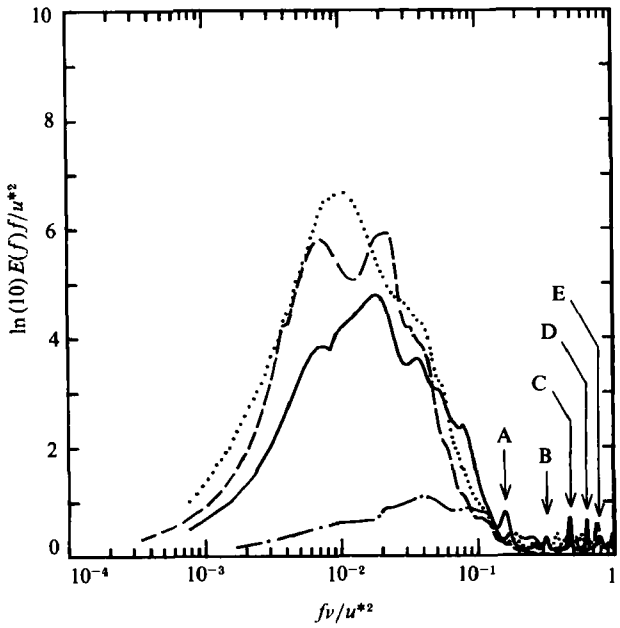

FIGURE 8. Spectra of streamwise velocity fluctuations at $y^+ = 15$ for F236 ($h = 15$ mm and $p = 63.5$ mm). —·—, $h^+ = 20.7$; ——, 31.5; ·····, 71.0; – – –, channel flow. In case $h^+ = 31.5$, the multiples of $1/T_p^+$ are shown as: A, $1/T_p^+$; B, $2/T_p^+$; C, $3/T_p^+$; D, $4/T_p^+$; E, $5/T_p^+$.

$\log_{10}(fv/u^{*2})$ should give the dimensionless streamwise fluctuation energy u'^2/u^{*2}; i.e.

$$\frac{u'^2}{u^{*2}} = \frac{1}{u^{*2}}\int_0^\infty E(f)\,\mathrm{d}f = \int_0^\infty \frac{E(f)}{\nu}\mathrm{d}\left(\frac{f\nu}{u^{*2}}\right)$$
$$= \int_{-\infty}^{\infty} \frac{\ln(10)E(f)f}{u^{*2}}\mathrm{d}\left\{\log_{10}\left(\frac{f\nu}{u^{*2}}\right)\right\}. \tag{3.1}$$

The spectrum for $h^+ = 71.0$ agrees well with that for the channel flow. The spectra for $h^+ = 37.2$, 49.3, and 56.9 merge with the foregoing two spectra, though, for the sake of clarity, they are omitted from the figure. The spectral density for $h^+ = 31.5$ is slightly smaller, and that for $h^+ = 20.7$ is conspicuously diminished.

All the spectra except that of the channel flow have small peaks in the high-frequency range. These peaks correspond to the pulse-like fluctuations mentioned previously in the discussion of figure 7 and are located exactly at the frequencies of multiples of $1/T_p^+$ (for the case of $h^+ = 31.5$, these frequencies are shown in the figure). It is clearly observed that these peaks contribute little to the fluctuation energy. Thus the basic structure of the wall turbulence is considered to remain virtually unchanged except in the case of $h^+ = 20.7$.

3.5. *Other combinations of h and p*

So far the results for series F236 ($h = 15$ mm and $p = 63.5$ mm) have been presented. Similar results were obtained for the cases of F315 ($h = 20$ mm and $p = 63.5$ mm) and F118 ($h = 15$ mm and $p = 127$ mm). In case F039 ($h = 5$ mm and $p = 127$ mm),

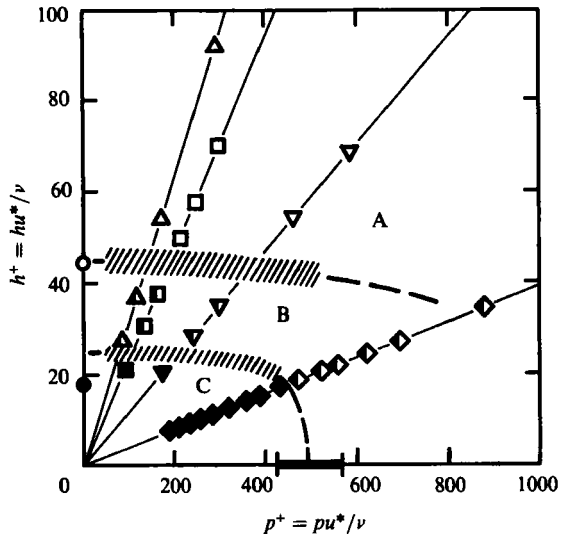

FIGURE 9. Flow-regime map in the (h^+, p^+)-plane: open symbols in region A are 'fully turbulent', half-solid symbols in region B 'transitional', and solid symbols in region C 'laminar-like'; △, F315 ($h = 20$ mm and $p = 63.5$ mm); □, F236 (15 mm and 63.5 mm); ▽, F118 (15 mm and 127 mm); ◇, F039 (5 mm and 127 mm).

the traverse of the hot-film probe was practically impossible within the limited vertical space of h; thus, the velocity fluctuations were measured at a fixed point of $y = 1.6$ mm.

4. Discussion

As described in the first part of §3, the experimental points are plotted in the (h^+, p^+)-plane, which specifies the degree of spatial restriction, and are distinguished by the state of the flow (figure 9). The experimental points under a fixed combination of h and p are on a straight line as illustrated in figure 3. Thus the four experimental series in this study describe the four respective lines in figure 9.

In the three cases F315 ($h = 20$ mm and $p = 63.5$ mm), F236 ($h = 15$ mm and $p = 63.5$ mm), and F118 ($h = 15$ mm and $p = 127$ mm), the state of the flow was divided into three kinds. The behaviour of the flow for a large h^+ could not be distinguished from the fully developed wall turbulence, and is labelled 'fully turbulent' in figure 9. For a moderate h^+, the mean velocity profile fell between those of fully turbulent and laminar flows, while the turbulent-intensity distribution took only a slightly smaller value than that of the fully turbulent flow. Such a case is labelled 'transitional'. When h^+ was small, the mean velocity profile became almost linear and the turbulent-intensity distribution diminished greatly. This case is referred to as 'laminar-like'. In case F039 ($h = 5$ mm and $p = 127$ mm), measurement at a fixed vertical position and its spectral analysis offered appreciable information to distinguish the state of the flow as 'laminar-like' or 'transitional'.

The abscissa of figure 9 represents the limiting case of $h \to 0$, where the flow is confined in each space bounded by two neighbouring fences. Koseff & Street (1984) performed an experiment on lid-driven cavity flow. This is exactly equivalent to

the case of $h \to 0$. They observed that certain perturbations began to appear at $Re_p = pU_c/\nu = 6000$–8000. This observation concerned the secondary eddy formed at the upstream corner of the cavity, while the flow structure near the moving wall, which seemed more stable than the secondary eddy, was not referred to in their report. We assume that the flow near the moving wall is laminar at least up to the Reynolds number given above. Here, p^+ is expressed as

$$p^+ = \frac{pu^*}{\nu} = \frac{pU_c}{\nu}\frac{u^*}{U_c} = Re_p(\tfrac{1}{2}C_f)^{\frac{1}{2}}, \tag{4.1}$$

where C_f is the friction coefficient $2\tau_w/\rho U_c^2$. Substituting the foregoing values of Re_p and assuming $C_f \approx 0.01$ yields $p^+ = 420$–570. This range is assumed to be the possible least bound of the boundary between the laminar-like and transitional regimes and is shown as a bold segment on the abscissa in figure 9.

In the limit where the experimental point approaches the ordinate of figure 9, on the other hand, a kind of Couette flow is thought to be realized. In the case of pure Couette flow, however, the boundary layers develop from both wall surfaces. Then, h in the present investigation may be equivalent to half the distance between the two boundary walls of the pure Couette flow. El Telbany & Reynolds (1982) have reviewed the experimental relation between the friction coefficient C_f and the Reynolds number Re_h of Couette flow, where C_f and Re_h are based on the centreline velocity and half the distance between the plates. The lower and upper boundary points of the laminar–turbulent transition regime were read from their correlation diagram and were substituted into the following counterpart of (4.1):

$$h^+ = Re_h(\tfrac{1}{2}C_f)^{\frac{1}{2}}. \tag{4.2}$$

The numerical values are: for the lower boundary, $Re_h = 320$, $C_f = 0.006$, and $h^+ = 17.5$ and for the upper boundary, $Re_h = 700$, $C_f = 0.008$, and $h^+ = 44.3$. These values of h^+ are shown as solid and open circles on the ordinate in figure 9.

Thus we have obtained a regime map of the fully turbulent, transitional and laminar-like flows in the (h^+, p^+)-plane, though there remains some uncertainty in the scope of the present experimental data. Where the non-dimensional pitch p^+ is less than 500, the turbulent structure near the wall is not influenced by the fences so long as the vertical extent from the wall h^+ is about 45, whereas the turbulent structure is no longer maintained when the vertical extent h^+ becomes less than about 25. These values of the vertical extent needed for the structure near the wall to be maintained are considered to be the fundamental vertical scales of the wall turbulence, and it turns out that they correspond well to the estimated height of the counter-rotating eddy pairs mentioned in §1 (Blackwelder 1983).

Experiments in which p^+ is changed and h^+ is kept sufficiently small, would reveal the streamwise extent needed to maintain the inner-layer structure of wall turbulence. We shall investigate in this direction in the future work.

5. Conclusions

Shear flow between a flat plate and a moving plate fitted with tall fences was investigated with hot-film anemometry. The boundary layer developing on the flat-plate side was subjected to the spatial restriction imposed by the tips of the fences, and the response of the inner layer of the boundary layer to the interference

was examined. Even when the tips of the fences were passing at a distance $y^+ = 45$ from the flat plate, the basic structure of the inner layer was little affected. The flow did not become laminar-like until the tips reached $y^+ = 25$. These results suggest that provided that the spatial extent of $45\nu/u^*$ from the wall is ensured, the inner layer develops a tough, self-sustaining structure which is uniquely determined under a given mean wall shear stress, and that this structure is hardly influenced by outer-layer disturbances, though the inner layer does interact with the outer layer through production of Reynolds stress. This statement receives further support from the flow-regime map in the non-dimensional plane of the free vertical space from the wall h^+ versus the longitudinal pitch of the fences p^+. The vertical extent of $h^+ = 45$ corresponds well to the estimated height of the counter-rotating eddy pairs in the literature.

The authors thank Mr Hiroshi Sukegawa for his efforts in designing and constructing the experimental apparatus, and Mr Koji Dozaki, Mr Noriaki Kohno and Mr Toru Masaki for their help in the experiments.

REFERENCES

ALFREDSSON, P. H. & JOHANSSON, A. V. 1984 On the detection of turbulence-generating events. *J. Fluid Mech.* **139**, 325.

ANDREOPOULOS, J., DURST, F., ZARIC, Z. & JOVANOVIC, J. 1984 Influence of Reynolds number on characteristics of turbulent wall boundary layers. *Exps Fluids* **2**, 7.

BAKEWELL, H. P. & LUMLEY, J. L. 1967 Viscous sublayer and adjacent wall region in turbulent pipe flow. *Phys. Fluids* **10**, 1880.

BLACKWELDER, R. F. 1983 Analogies between transitional and turbulent boundary layers. *Phys. Fluids* **26**, 2807.

BLACKWELDER, R. F. & ECKELMANN, H. 1979 Streamwise vortices associated with the bursting phenomenon. *J. Fluid Mech.* **94**, 577.

BLACKWELDER, R. F. & HARITONIDIS, J. H. 1983 Scaling of the bursting frequency in turbulent boundary layers. *J. Fluid Mech.* **132**, 87.

BLACKWELDER, R. F. & KAPLAN, R. E. 1976 On the wall structure of the turbulent boundary layer. *J. Fluid Mech.* **76**, 89.

BRODKEY, R. S., WALLACE, J. M. & ECKELMANN, H. 1974 Some properties of truncated turbulence signals in bounded shear flows. *J. Fluid Mech.* **63**, 209.

BROWN, G. L. & THOMAS, A. S. W. 1977 Large structure in a turbulent boundary layer. *Phys. Fluids* **20**, S243.

CORINO, E. R. & BRODKEY, R. S. 1969 A visual investigation of the wall region in turbulent flow. *J. Fluid Mech.* **37**, 1.

DINKELACKER, A., HESSEL, M., MEIER, G. E. A. & SCHEWE, G. 1977 Investigation of pressure fluctuations beneath a turbulent boundary layer by means of an optical method. *Phys. Fluids* **20**, S216.

ECKELMANN, H. 1974 The structure of the viscous sublayer and the adjacent wall region in a turbulent channel flow. *J. Fluid Mech.* **65**, 439.

EL TELBANY, M. M. M. & REYNOLDS, A. J. 1982 The structure of turbulent plane Couette flow. *Trans. ASME* I: *J. Fluids Engng* **104**, 367.

FALCO, R. E. 1977 Coherent motions in the outer region of turbulent boundary layers. *Phys. Fluids* **20**, S124.

FLEISCHMANN, S. T. & WALLACE, J. M. 1984 Mean streamwise spacing of organized structures in transitional and developed bounded turbulent flows. *AIAA J.* **22**, 766.

GUPTA, A. K. & KAPLAN, R. E. 1972 Statistical characteristics of Reynolds stress in a turbulent boundary layer. *Phys. Fluids* **15**, 981.

HIRATA, M., TANAKA, H., KAWAMURA, H. & KASAGI, N. 1982 Heat transfer in turbulent flows. In *Proc. 7th Intl Heat Transfer Conf., Munich* (ed. U. Grigull, E. Hahne, K. Stephan & J. Straub), vol. 1, p. 31. Hemisphere.

IRITANI, Y., KASAGI, N. & HIRATA, M. 1983 Heat transfer mechanism and associated turbulence structure in the near-wall region of a turbulent boundary layer. In *Proc. 4th Symp. Turbulent Shear Flows, Karlsruhe*, p. 17.31. Springer.

JOHANSSON, A. V. & ALFREDSSON, P. H. 1983 Effects of imperfect spatial resolution on measurements of wall-bounded turbulent shear flows. *J. Fluid Mech.* **137**, 409.

KIM, H. T., KLINE, S. J. & REYNOLDS, W. C. 1971 The production of turbulence near a smooth wall in a turbulent boundary layer. *J. Fluid Mech.* **50**, 133.

KLINE, S. J., REYNOLDS, W. C., SCHRAUB, F. A. & RUNSTADLER, P. W. 1967 The structure of turbulent boundary layers. *J. Fluid Mech.* **30**, 741.

KOSEFF, J. R. & STREET, R. L. 1984 Visualization studies of a shear driven three-dimensional recirculating flow. *Trans. ASME* I: *J. Fluids Engng* **106**, 21.

KREPLIN, H. P. & ECKELMANN, H. 1979 Propagation of perturbations in the viscous sublayer and adjacent wall region. *J. Fluid Mech.* **95**, 305.

LAUFER, J. & BADRI NARAYANAN, M. A. 1971 Mean period of the turbulent production mechanism in a boundary layer. *Phys. Fluids* **14**, 182.

LEE, M. K., ECKELMAN, L. D. & HANRATTY, T. J. 1974 Identification of turbulent wall eddies through the phase relation of the components of the fluctuating velocity gradient. *J. Fluid Mech.* **66**, 17.

MEEK, R. L. 1972 Mean period of fluctuations near the wall in turbulent flows. *AIChE J.* **18**, 854.

MEEK, R. L. & BAER, A. D. 1970 The periodic viscous sublayer in turbulent flow. *AIChE J.* **16**, 841.

OLDAKER, D. K. & TIEDERMAN, W. G. 1977 Spatial structure of the viscous sublayer in drag-reducing channel flows. *Phys. Fluids* **20**, S133.

RAO, K. N., NARASIMHA, R. & BADRI NARAYANAN, M. A. 1971 The 'bursting' phenomenon in a turbulent boundary layer. *J. Fluid Mech.* **48**, 339.

SMITH, C. R. & METZLER, S. P. 1983 The characteristics of low-speed streaks in the near-wall region of a turbulent boundary layer. *J. Fluid Mech.* **129**, 27.

TANAKA, H. & YABUKI, H. 1986 Laminarization and reversion to turbulence of low Reynolds number flow through a converging to constant area duct. *Trans. ASME* I: *J. Fluids Engng* **108**, 325.

WALLACE, J. M., ECKELMANN, H. & BRODKEY, R. S. 1972 The wall region in turbulent shear flow. *J. Fluid Mech.* **54**, 39.

WILLMARTH, W. W. & LU, S. S. 1972 Structure of the Reynolds stress near the wall. *J. Fluid Mech.* **55**, 65.

WILLMARTH, W. W. & SHARMA, L. K. 1984 Study of turbulent structure with hot wires smaller than the viscous length. *J. Fluid Mech.* **142**, 121.